DOI: 10.3217/978-3-99161-057-1-158

Advancing high-fidelity Digital Twin Technology for Structural Health Monitoring

Ihar Antonau[1,2], Suneth Warnakulasuriya[3], Talhah Ansari[3,6], Roland Wüchner[3], Rainald Löhner[4,6], Facundo Nicolas Airaudo[4], Habir Antil[5]
[1]Cluster of Excellence SE[2]A -- Sustainable and Energy-Efficient Aviation, Technische Universität Braunschweig, Germany, www.tu-braunschweig.de/en/se2a
[2]Institute of Structural Analysis, Technical University of Braunschweig, Beethovenstrasse 51, 38106, Braunschweig, Germany
[3]Chair of Structural Analysis, Technical University of Munich, Arcisstr. 21, 80333, Munich, Germany
[4]Center for Computational Fluid Dynamics and Department of Physics and Astronomy, George Mason University, Fairfax, VA 22030, USA
[5]Center for Mathematics and Artificial Intelligence (CMAI) and Department of Mathematical Sciences, George Mason University, Fairfax, VA 22030, USA
[6]Institute for Advanced Study, Technical University of Munich, Lichtenbergstr. 2a, 85748 Garching, Germany
email: ihar.antonau@tu-braunschweig.de, suneth.warnakulasuriya@tum.de, talhah.ansari@tum.de, wuechner@tum.de, fairaudo@gmu.edu, rlohner@gmu.edu, hantil@gmu.edu

ABSTRACT: This study addresses the need for high-fidelity system identification in Digital Twin (DT) applications for Structural Health Monitoring (SHM). As infrastructure ages, its material properties may degrade due to various factors, including damage, corrosion, and fatigue. Accurate assessment of material properties is critical for ensuring safety and reliability. High-fidelity identification enables the detection of localized damages that traditional methods may not detect, directly impacting maintenance strategies and public safety. In this work, we present a formulation of the optimization problem that minimizes errors between observed and simulated displacements by varying material properties. Additionally, we utilize adjoint-based sensitivity analysis, combined with regularization techniques such as Vertex Morphing, to enhance the efficiency and robustness of the optimization process. Our case studies, which include detailed analyses of 2D and 3D structures using real-world data, demonstrate the effectiveness of our methods in accurately inferring material properties and revealing structural integrity. By implementing this advanced methodology, practitioners can achieve timely and accurate assessments of structural integrity, leading to better-informed decision-making regarding maintenance and safety protocols. This research contributes to the ongoing advancement of Digital Twin technology, promoting safer and more efficient infrastructure management.

KEYWORDS: High-fidelity Digital Twin, Inverse Problems, Regularization, Adjoint sensitivity analysis.

1 INTRODUCTION

Throughout the lifecycle of structures, their material properties can deteriorate due to various factors, including damage, corrosion, and fatigue. Advances in sensor technology and numerical simulation techniques now enable the creation of Digital Twins (DT) — dynamic digital representations of complex structures. DT can be defined as follows [7-10]:

"A set of virtual information constructs that mimic the structure, context, and behavior of an individual/unique physical asset, or a group of physical assets, is dynamically updated with data from its physical twin throughout its life cycle and informs decisions that realize value."

A key component in developing DT is system identification, which involves evaluating the current state of material properties and identifying areas of weakness. This process often requires solving inverse problems through appropriate parameterization, typically framed as an optimization challenge. The formulation steps of the system identification problem can be outlined as follows:

1. *System Description*: Analyze all available information about physical objects and numerical models, including documentation, numerical models, or data from the design phase, for instance, testing data from wind tunnels or experiments with material samples.
2. *State Information*: Collect and analyze available sensor data, measurements, load tests, and visual inspections to inform the assessment.
3. *Definition of Optimization Problem*: Define the objective function that incorporates the available measured data and select system parameters to minimize the errors between measured and computed data points.

Figure 1 illustrates the "twinning" process schematically. In real-world applications, the structure can be used under various conditions. A digital model can predict performance and provide feedback about the structure, indicating whether it requires maintenance or can be safely used further. To enhance the feedback provided by the digital model, the system identification process aligns the real and virtual worlds.

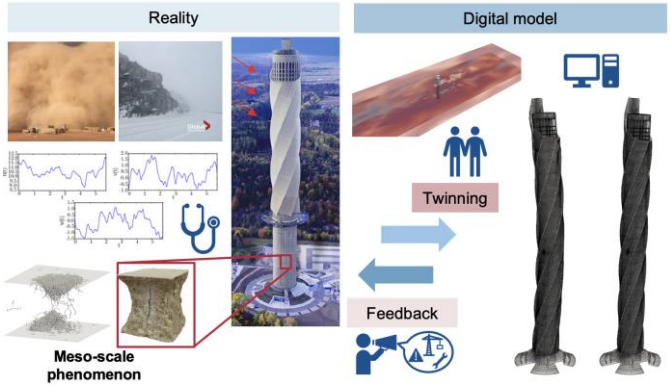

Figure 1. Twinning real and digital worlds.

DOI: 10.3217/978-3-99161-057-1-158

In system identification, various fidelities can be applied, which can be categorized into two main types: analysis and identification, as shown in Figure 2. Low-fidelity analysis is represented by simplified finite element (FE) models, such as using beam elements to describe the structure. In contrast, high-fidelity models incorporate detailed geometry, complex material laws, and other intricate characteristics.

Similarly, low-fidelity identification involves a limited number of parameters that typically reflect the overall structural behavior of the system. Low-fidelity system identification is well solved using artificial neural networks. For instance, in [14], the identification parameters are the coordinates of the damaged regions and the stiffness reduction factor. This setup allows for the localization of damage, but it is limited to a single region. In [16], the three-floor structure is studied, where each floor has its own set of global identification parameters, which describe the structure's properties. As a result the damage localization is limited to the floor.

In high-fidelity identification, however, many system parameters need to be determined, for example, a unique set for each finite element in the model. Consequently, while low-fidelity identification can indicate an average weakening in the structure, high-fidelity identification can localize many damaged regions with different shapes and damage intensity.

In this work, we focus on high-fidelity FE models and high-fidelity identification as the most challenging case. However, the proposed methodology can also be applied to other fidelity cases.

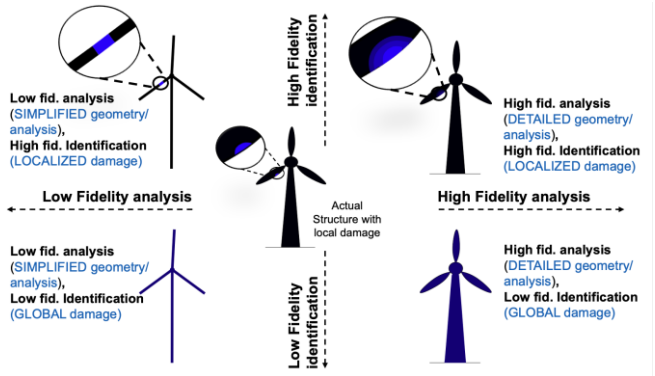

Figure 2. Fidelity levels in the FE model and system identification.

An adjoint analysis is an essential component of solving high-fidelity system identification problems with many parameters. The adjoint-based technique for localizing damages in structures using displacement and strain measurements is presented in [1]. A combination of several sensor approaches would also appear highly promising in future applications [11], including risk measures and uncertainty quantification [12]. Additionally, recent research has demonstrated the potential for restoring the temperature field based on displacement and strain measurements [13].

Frequent updates between numerical and physical assets are an essential property of the digital twin in practical applications. Live monitoring requires a fast solution to the system identification problem to analyze and update the system. In [3], the authors studied the possible computational cost reduction using various optimization algorithms.

This study addresses the minimization problem associated with identifying material properties within numerical models. The cost function is formulated based on the aggregated errors between observed and simulated displacements across multiple locations. To enhance the robustness of the minimization process, we employ various smoothing and filtering techniques, including the Vertex Morphing approach, which helps regularize the optimization problem.

We present both 2D and 3D structural case studies, where one of the cases are represented by a testing bridge “Concerto”. Our examples utilize real-world data alongside numerical simulations to demonstrate the effectiveness of our methods in accurately inferring material properties and revealing structural integrity. This work contributes to the ongoing advancement of Digital Twin technology for effective structural health monitoring, ultimately promoting safer and more reliable infrastructure.

2 METHODOLOGY

The system identification of material properties, such as damage, can be formulated as an optimization problem involving unknown material parameters $\boldsymbol{p} = [p_1, p_2, \dots p_n]$. Depending on the applied material model, the unknown material parameters can be Young's modulus, Poisson's ratio, or other, at each of the elements in the finite element model (FEM). Figure 3 illustrates the components of generalized system identification, which includes a digital twin and the optimization problem.

The digital twin comprises a physical object, measured data, and a numerical model. The key components of the optimization process are material parameters, a regularization technique, an optimization algorithm, and the formulation of the objective function, which incorporates the available measured data. The following sections describe details of each component and its challenges.

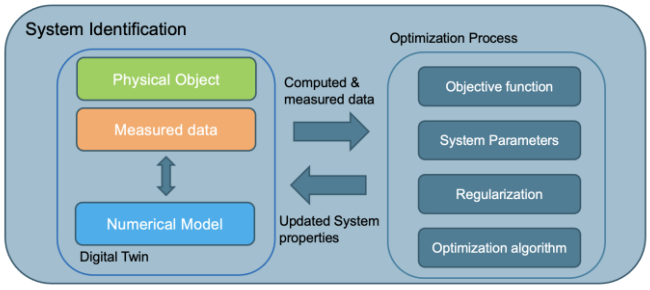

Figure 3. System identification process.

2.1 Objective function

One of the key components in setting up the optimization process is defining the objective function. Based on the available data, the generalized objective function can be formulated as a weighted sum of the errors between measured and computed quantities. Given l number of the different sensor types and n given load cases $\boldsymbol{F}_i, i = 1..n$; $n \cdot l$ corresponding measurements at m measuring points of their respective data φ. The variable φ can represent different quantities based on the sensor type, for instance, displacement, strain, temperature, acceleration and etc. The generalized objective (cost) function is formulated as:

DOI: 10.3217/978-3-99161-057-1-158

$$J\left(\boldsymbol{p}, \boldsymbol{\varphi}(\boldsymbol{p})\right) = \sum_{k=1}^{l}\sum_{i=1}^{n}\sum_{j=1}^{m} \Phi\left(\omega_{kij}, \boldsymbol{\varphi}_{kij}^{md}, \underline{\boldsymbol{I}}_{\boldsymbol{kij}}^{\boldsymbol{d}}\boldsymbol{\varphi}_{\boldsymbol{ki}}(\boldsymbol{p}), \boldsymbol{p}\right) \quad (1)$$

where ω_{kij} are the measurement weights; $\underline{\boldsymbol{I}}_{\boldsymbol{kij}}^{\boldsymbol{d}}$ are interpolation matrices that are used to obtain the computed value from the finite element mesh at the measurement locations. $\Phi\left(\omega_{\mathrm{kij}}, \boldsymbol{\varphi}_{\mathrm{kij}}^{\mathrm{md}}, \underline{\mathbf{I}}_{\mathrm{kij}}^{\mathrm{d}}\boldsymbol{\varphi}_{\mathrm{ki}}(\mathbf{p})\right)$ is a weighted aggregation function, for instance, weighted square sum:

$$\Phi = \frac{1}{2}\omega_{kij}\left[\boldsymbol{\varphi}_{\boldsymbol{kij}}^{md} - \underline{\boldsymbol{I}}_{\boldsymbol{kij}}^{\boldsymbol{d}}\boldsymbol{\varphi}_{\boldsymbol{ki}}(\boldsymbol{p})\right]^2 \quad (2)$$

In case, only one load case is considered with one sensor type with displacement measurements, and the material parameter of interest is Young's modulus, then the objective function defined in Equation (1) simplifies to:

$$J\left(\boldsymbol{u}(\boldsymbol{E})\right) = \frac{1}{2}\sum_{j=1}^{m}\omega_j\left(\boldsymbol{u}_{\boldsymbol{j}}^{md} - \underline{\boldsymbol{I}}_{\boldsymbol{j}}^{\boldsymbol{d}}\boldsymbol{u}(\boldsymbol{E})\right)^2 \quad (3)$$

2.2 Sensitivity analysis

An important step in the optimization process for identifying material parameters is computing the derivative of the objective function with respect to the material parameters. Considering the objective function introduced in Equation (3), we can apply the chain rule:

$$\frac{dJ}{d\boldsymbol{E}} = \frac{\partial J}{\partial \boldsymbol{E}} + \frac{\partial J}{\partial \boldsymbol{u}}\frac{d\boldsymbol{u}}{d\boldsymbol{E}} \quad (4)$$

where $\frac{\partial J}{\partial \boldsymbol{E}} = 0$ because J does not depend directly on $\boldsymbol{E}$, Equation (4) can be further developed:

$$\frac{dJ}{d\boldsymbol{E}} = \frac{\partial J}{\partial \boldsymbol{u}}\frac{d\boldsymbol{u}}{d\boldsymbol{E}} = -\left(\sum_{j=1}^{m}\omega_j\left(\boldsymbol{u}_{\boldsymbol{j}}^{md} - \underline{\boldsymbol{I}}_{\boldsymbol{j}}^{\boldsymbol{d}}\boldsymbol{u}\right)\right)\frac{d\boldsymbol{u}}{d\boldsymbol{E}} \quad (5)$$

In general, $\frac{dJ}{d\boldsymbol{E}}$ can be computed using either the finite difference approach or the adjoint approach. Due to a large number of material parameters to identify, the adjoint approach is preferred because it is computationally more efficient by avoiding the direct computation of $\frac{d\boldsymbol{u}}{d\boldsymbol{E}}$. Adjoint approach requires first solving a primal problem, which is depicted in Equation (6) in the residual form, where $\boldsymbol{K}$ is the stiffness matrix, $\boldsymbol{u}$ is the displacement vector, and $\boldsymbol{F}$ is the load vector:

$$\boldsymbol{R} = \boldsymbol{K}\boldsymbol{u} - \boldsymbol{F} \quad (6)$$

Then, the adjoint problem is solved for $\boldsymbol{\lambda}$ Lagrange multipliers:

$$\left(\frac{\partial \boldsymbol{R}}{\partial \boldsymbol{u}}\right)^T\boldsymbol{\lambda} = -\left(\frac{\partial J}{\partial \boldsymbol{u}}\right)^{\mathrm{T}} \quad (7)$$

and the Lagrange multipliers are used in a post-processing step to compute the final sensitivities:

$$\frac{dJ}{d\boldsymbol{E}} = \frac{\partial J}{\partial \boldsymbol{E}} + \boldsymbol{\lambda}^T\frac{\partial \boldsymbol{R}}{\partial \boldsymbol{E}} \quad (8)$$

We would like to note that the Equation (7) is independent of the choice of the material parameter. Hence, the adjoint approach can be used for various material parameters and Young's modulus $\boldsymbol{E}$ has been used as an example. A lot of performance and implementation optimization can be achieved by solving the adjoint system, because $\left(\frac{\partial \boldsymbol{R}}{\partial \boldsymbol{u}}\right)^T = \boldsymbol{K}^T$ and $\boldsymbol{K}$ is symmetric, hence we can re-use the existing left-hand side of the primal problem and only have to change the right-hand side (i.e. pseudo-load)to obtain $\boldsymbol{\lambda}$.

2.3 Regularization

Similarly to node-based shape and topology optimization, to avoid high-frequency noisy results, we need to apply appropriate regularization techniques [2]. Therefore, one option is to subject the raw gradients to smoothing using filters. In [1], the authors reviewed various gradient smoothing techniques for material identification problems, such as simple element averaging, weak Laplacian smoothing, and pseudo-Laplacian smoothing, where the last one has been chosen as a better technique. In [3], the authors apply an explicit filter called Vertex Morphing to smooth material gradients. In the context of Vertex Morphing, thus, the physical material properties, for instance, Young's Modulus $\boldsymbol{E}$ are indirectly controlled by an unsmoothed control field $\boldsymbol{p}$ and a kernel (or filter) function $\mathcal{F}$, for example, on the surface Γ with surface coordinates (ξ, η, ζ):

$$(\xi_0, \eta_0, \zeta_0) = \int_{\Gamma}\mathcal{F}\left(\xi - \xi_0, \eta - \eta_0, \zeta - \zeta_0\right)\boldsymbol{s}(\xi, \eta, \zeta)d\Gamma \quad (9)$$

After discretization of the structural geometry $\boldsymbol{E} = [E_1, E_2, \ldots, E_n]$ and control function $\boldsymbol{s} = [s_1, s_2, \ldots, s_n]$ by standard techniques such as the finite element method, Vertex Morphing appears as:

$$\boldsymbol{E} = \underline{\boldsymbol{A}}\boldsymbol{s} \quad (10)$$

Where $\boldsymbol{E}$ is Young's modulus of elements, and they are arranged sequentially. $\underline{\boldsymbol{A}}$ is the filter operator matrix, and $\boldsymbol{s}$ is the vector of discrete control field parameters, again arranged sequentially. The most straightforward approach is to add control parameters to every element.

The entries A_{ij} of the filter matrix $\underline{\boldsymbol{A}}$ reflect the filter effect as the interaction between two different centers of the elements i and j, their center's spatial position vectors x_i and x_j, and their Euclidean distance $\|x_i - x_j\|$. For the case of the Gauss distribution as kernel function and approximating integration by summation, it holds:

$$A_{ij} = \mathcal{F}\left(x_i, x_j\right)/sum$$
$$sum = \sum_{j}\mathcal{F}\left(x_i, x_j\right) \quad (11)$$

$$\mathcal{F}\left(x_i, x_j\right) = \begin{cases} e^{-\|x_i - x_j\|^2/2r^2}, \|x_i - x_j\| \le r \\ 0.0, \|x_i - x_j\| > r \end{cases} \quad (12)$$

and r is the filter radius. By changing the filter radius, one can adjust the filtering intensity.

2.4 Generalized workflow

Figure 4 shows the generalized workflow of the optimization process for system identification. Every optimization iteration, we need to evaluate objective function value and it's gradients. Then, we apply Vertex Morphing (or other filtering technique) on the computed gradients and compute the control parameter update using optimization algorithm. Then, we apply one more time Vertex Morphing on the computed control parameter update to compute new model parameters state. This process continues till the convergence criteria are met or maximum number of optimization iterations are reached.

DOI: 10.3217/978-3-99161-057-1-158

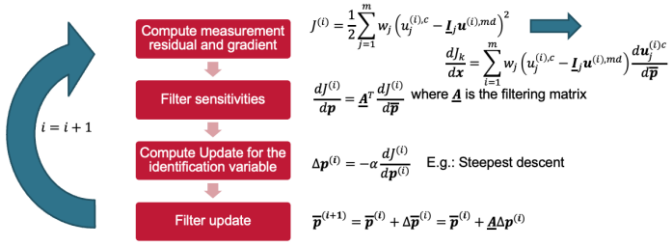

Figure 4. Generalized system identification workflow as an optimization process.

Relevant optimization convergence criteria for system identification are:

1. Relative reduction of objective function:

$$\frac{J(\boldsymbol{p}^i)}{J(\boldsymbol{p}^0)} \leq \varepsilon \tag{13}$$

2. Absolute reduction of objective function:

$$J(\boldsymbol{p}^0) - J(\boldsymbol{p}^i) \geq \varepsilon \tag{14}$$

3. Maximum sensor error:

$$\max_j abs(\boldsymbol{u}_j^{md} - \underline{\boldsymbol{I}}_j^{\boldsymbol{d}}\boldsymbol{u}(\boldsymbol{p})) \leq \varepsilon \tag{15}$$

In general, a lot of standard techniques from optimization theory can be apply to solve system identification problems, including convergence criteria, optimization algorithms, aggregation techniques, variable scaling, line search techniques and globalization strategies.

3 CHALLENGES IN SYSTEM IDENTIFICATION

In this section main challenges of the method are summarized.

3.1 Modeling the objective function

The choice of the objective can play a crucial role in system identification because various types of measured data have to be combined. That require a proper scaling of the measured information to keep the objective function dimensionless and it allows to find a "correct" solution. Additionally, in minimization of the sum of the errors, the component with the highest error would have the highest contribution to the search direction. The sensor with highest error may change in the sequential optimization iterations leading to zig-zagging behavior. In [1], authors reviewed few weighting strategies to combine strains and displacements. In case of Equation (3), these techniques compute weights for displacements as follows:

1. *local weighting:*

$$\omega_j = \left(\boldsymbol{u}_j^{md}\right)^{-2}$$

This method may lead to an 'over-emphasis' of small displacements, that are in regions of marginal interest.

2. *average weighting:*

$$\omega_j = \left[\frac{\sum_{j=1}^{m}\left|\boldsymbol{u}_j^{md}\right|}{m}\right]^{-2}$$

This method may lead to an 'under-emphasis' of small displacements that may occur in important regions.

3. *max weighting:*

$$\omega_j = \left[\max_j\left|\boldsymbol{u}_j^{md}\right|\right]^{-2}$$

This method may lead to an 'under-emphasis' of smaller displacements that can occur in important regions;

4. *local/max weighting:*

$$\omega_j = \max\left[\varepsilon \max_j\left|\boldsymbol{u}_j^{md}\right|, \left|\boldsymbol{u}_j^{md}\right|\right]^{-2}$$

where $\varepsilon = [0.01, 0.1]$. This method works best of all, as it combines local weighting with a max-bound minimum for local values.

The weights for strain components (or other measured values) can be computed in a similar manner.

3.2 Large design space

In our approach, we aim to identify the material parameters for each element individually. As a result, there are various spatial distributions of material properties that can produce similar or identical deformations under a fixed load case. This type of optimization problem is known as "multimodal," meaning it has multiple optimal solutions with the same objective function values. Consequently, engineering expertise is necessary to "narrow" down the design space. For example, if the material is expected to weaken over time, we can impose an upper limit on Young's modulus to prevent stiffening of the structure, as illustrated in Figure 5.

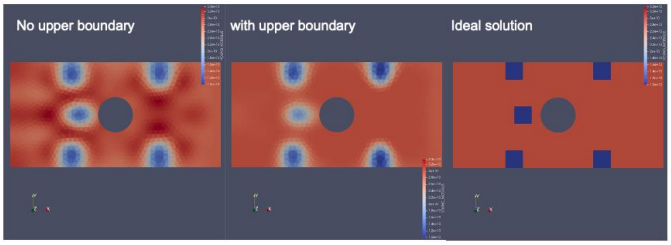

Figure 5. Results of the system identification problem with (right) and without (middle) stiffening in the material.

To improve the convergence of the system identification process, authors in [4] suggest using a zoom-in approach, where they start with a limited number of design variables and then gradually reparametrize the problem to zoom into the damaged region by switching from low-fidelity identification to high-fidelity. This approach improves the robustness of the method by better finding the weak areas globally and afterward identifying damages on a smaller scale.

3.3 Discrete gradients

To localize damage effectively, it is necessary to consider many material parameters, such as modifying Young's modulus for each element. This results in a large number of parameters and the need for gradient-based optimization algorithms. Consequently, adjoint analysis is essential. Section 2.2 discusses the use of adjoint analysis to compute the gradients of the objective function.

The gradients obtained through adjoint methods can be discrete and noisy, which may lead to high-frequency solutions. To address this issue, regularization techniques are required. One such technique is Vertex Morphing, which is introduced in Section 2.3. Figure 6 illustrates the effect of Vertex Morphing.

DOI: 10.3217/978-3-99161-057-1-158

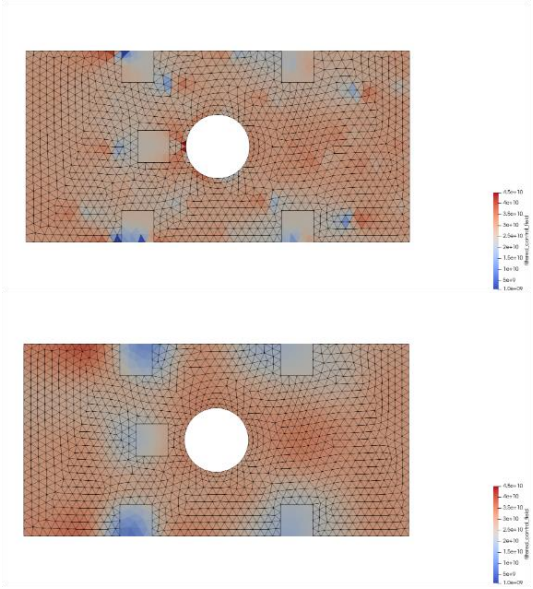

Figure 6. Young's Modulus distribution: top – without, bottom – with Vertex Morphing.

3.4 Optimization algorithm

The difference between classical mathematical optimization problem and system identification problem is that evaluation of the objective value typically requires solving the FEM-based structure analysis. Therefore, robust and efficient optimization algorithms are required with minimal functional and gradient evaluations. In [3], the authors compare various optimization algorithms and their performance. It has been shown that a significant amount of computational cost can be avoided by selecting a well-suited algorithm.

Figure 7 shows the performance of the various algorithms. 2D Plate with a hole (Section 4.1) has been used as a benchmark to study the performance. The tested algorithms are: SciPy Broyden-Fletcher-Goldfarb-Shanno (BFGS), SciPy Limited memory Broyden-Fletcher-Goldfarb-Shanno bounded algorithm (L-BFGS-B), SciPy conjugate gradient algorithm (CG), SciPy Trust-Region Constrained Algorithm (TRC), PyRol the steepest descent method with back-tracking line search, PyRol Lin-More trust region algorithm (LM-TR) and Kratos Nesterov accelerated gradient method with Quasi-Newton Barzilai-Borwein correction line search (NAG-QNBB).

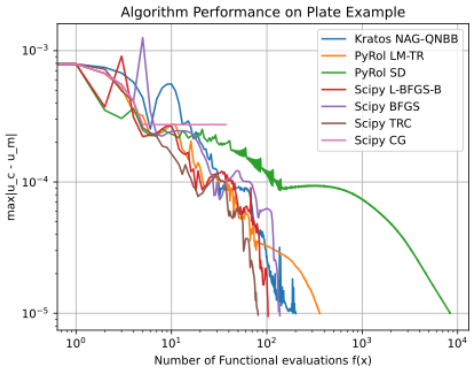

Figure 7. Convergence rate of the tested algorithms [3].

4 NUMERICAL EXAMPLES

This section demonstrates two examples of the system identification process. A simple 2D plate with a hole example is a numerical benchmark from [3], which is introduced to help the reader better understand the introduced methodology. The second example demonstrates the usability of the method on a real-world structure, and its measured performance is shown. The measured data were obtained from [5].

4.1 2D Plate with a hole

The FE model of the 2D plate with a hole is shown in Figure 8, where the left side is fixed, and the distributed force is applied on the right side. Figure 9 (left) shows displacements of the damaged model and the mapped displacements to the sensors. These displacements are used as "measured" displacements to identify the given damage. The virtual sensor is modeled as a point with x- and y- spatial coordinates, and the measured value is associated with its location. The damaged material is visible in Figure 9 (right).

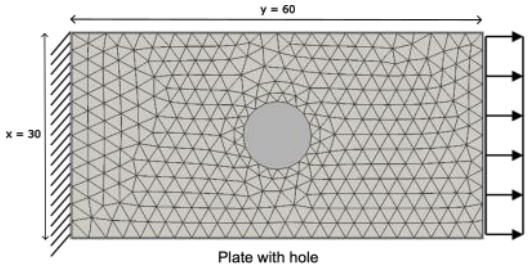

Figure 8. FEM model [3].

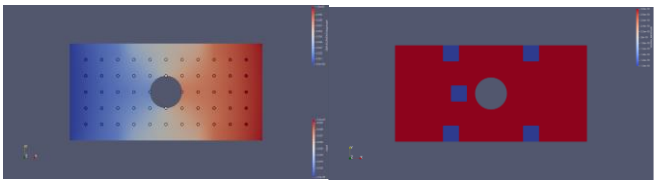

Figure 9. Measured displacements (left) and predefined damage (right) [3].

The objective function is defined similarly to Equation (3), and it is based on the measured and computed displacements in the x-direction:

$$J(\boldsymbol{u}(\boldsymbol{E})) = \frac{1}{2}\sum_{j=1}^{m} \omega_j \left(u_{x_j}^{md} - u_{x_j}(\boldsymbol{E})\right)^2 \qquad (16)$$

The filtering radius is chosen to be constant, and $r = 5$, covering approximately 4 FE elements. The optimization process stops when the maximum error in the sensor reaches 10^{-5}, Equation (15).

Figure 10 shows the found damaged areas using the system identification process. Due to the applied filtering, the found damage areas have smoothed boundaries in contrast to the ideal predefined damage model (Figure 9).

DOI: 10.3217/978-3-99161-057-1-158

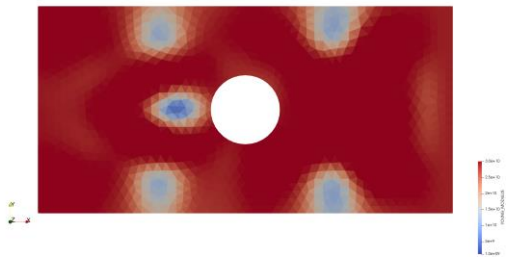

Figure 10. Found damaged areas using the NAG-QNBB algorithm [3]

4.2 Concerto bridge

For the long-term evaluation of innovative Structural Health Monitoring (SHM) techniques, the experimental plate girder bridge "Concerto" was constructed in 2005. The bridge measures 17.5 m in total length, 4.0 m in width, and 0.8 m in height [5, 6]. Figure 11 shows the support positions (A, B), the ground anchors (C), the transducers (C, D), and the cantilever arm (E). In the lower part of Figure 11, the instrumentation and reference point signalization are depicted.

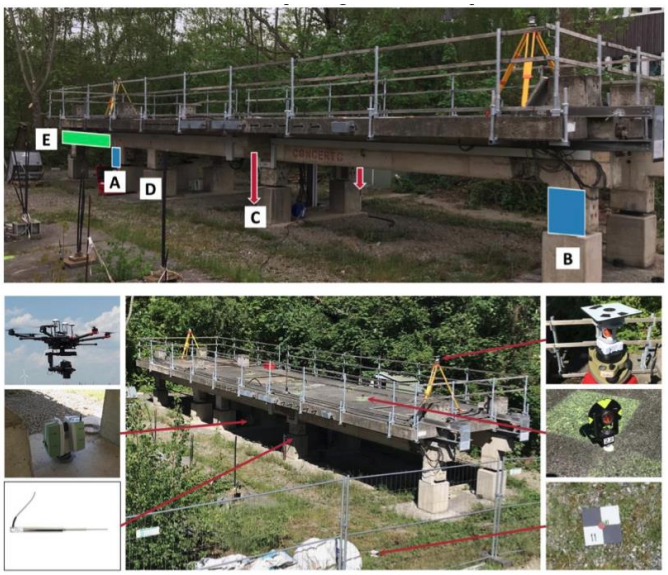

Figure 11. Experimental Bridge "Concerto". Upper part: indication of support (A, B), ground anchor (C), Deformation transducer positions (C and D), and cantilever arm (E). Lower part: instruments (UAV, laser scanner, and transducer) and signalization of reference points [5].

Figure 12 shows the deformation of the bridge under the load from photogrammetric measurements. For more details on the measurement techniques, an interested reader is referred to [5]. In this study, we utilized data obtained through photogrammetric measurements. However, data from other measurement techniques can also be applied. We chose photogrammetric measurements because they provide continuous data, in contrast to the limited number of points obtained from tachymetry and transducer measurements. It is important to note that laser scanner measurements exhibit a gap between 12.5 meters and 15 meters.

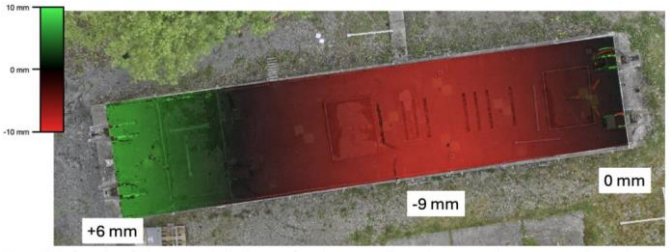

Figure 12. According to photogrammetric measurements, the deformation of "Concerto" under load is seen from the top. Lowered areas are colored in red, elevated areas in green, and no elevation change in black [5].

A finite element (FE) model has been created to model the bridge, as shown in Figure 13. This model consists of 77,000 small-displacement 3D elements that represent the concrete domain (depicted in gray), 800 truss elements representing the tendons (shown in blue), and 107 small-displacement 3D elements that represent the elastomers (illustrated in yellow). The load is applied to the red surfaces.

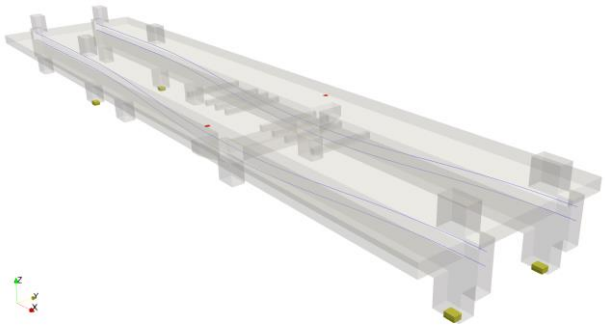

Figure 13. FE-model of the Concerto bridge: concrete part (gray), steel tendons (blue), elastomers (yellow), applied force (red).

To utilize the measured data, we create a series of virtual sensors positioned along the x-axis at the midpoint of the bridge. Figure 14 illustrates the locations of these virtual sensors, represented as spheres, along with their corresponding values (displacement in the z-direction) that have been derived from the measured data.
The objective function is defined similar to Equation (3) and it is based on the photogrammetric measurements and computed displacements in the z-direction:

$$J(\boldsymbol{u}(\boldsymbol{E})) = \frac{1}{2}\sum_{j=1}^{m} \omega_j \left(u_{z_j}^{md} - u_{z_j}(\boldsymbol{E})\right)^2 \qquad (17)$$

There are three various material domains to identify in the model. The largest domain is concrete, where we set the valid Young's modules range to $E = [1e9, 1e11]\ Pa$ and as the initial parameter $E^0 = 3e10\ Pa$. In this model, we set the upper boundary higher than the initial value because we want to keep large identification freedom. The second material domain is steel tendons, with parameter ranges $E = [1e10, 1e12]\ Pa$ and $E^0 = 2.1e11\ Pa$. The last model part is elastomers, which model the rubber supports with unknown material properties. We set $E = [1e6, 1e8] Pa$ and $E^0 = 1e7\ Pa$. All material

DOI: 10.3217/978-3-99161-057-1-158

parameters are identified through a single system identification process.

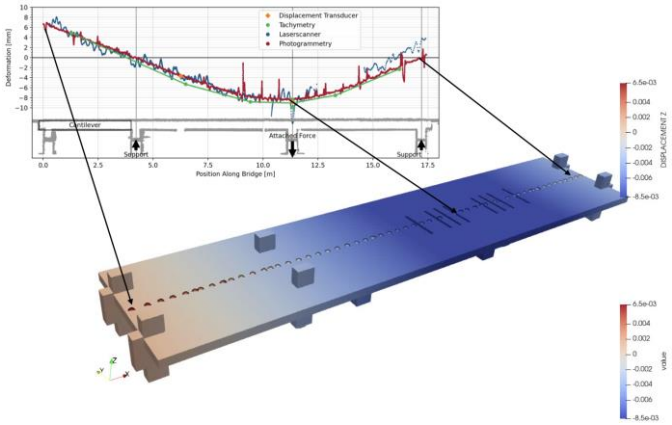

Figure 14. Applying the measured data to its numerical model: measured data at the center line (top graph), virtual sensors with mapped data (small circles).

Figure 15-18 shows the final Young's modulus of the materials. The results show that steel tendons are not damaged, and the elastomer material converges to $1e8\,Pa$. In Figure 16, we highlight the areas with damaged concrete and provide photos of these areas. Figure 17 shows the graph comparing the measured and computed displacement at the middle line before and after system identification.

Figure 15.Young's modulus of steel tendons shows no damage.

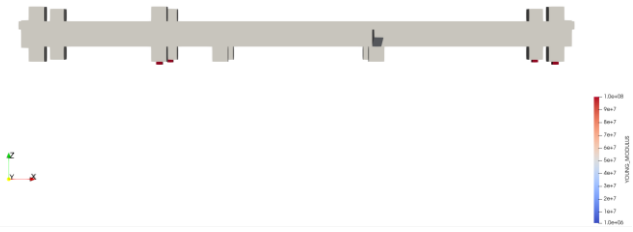

Figure 16.Young's modulus of elastomers converged to upper bound (1e8).

The optimization process took 30 optimization iterations to reduce the objective function by 98.9 %. Further optimization iterations lead to overfitting the parameters (see Figure 19), where the material parameters converge to unphysical values, while the reduction of the cost function stays at similar level 99.1 %.

Figure 17. Top: Young's modulus of concrete. Bottom: Pictures of the current state of the bridge in the weakened regions.

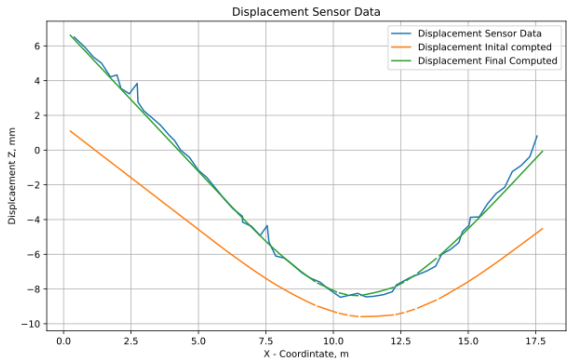

Figure 18. Comparing z-displacements along the x-axis in the middle of the bridge: measured data (green), initial computed data (orange), final computed data (blue).

Figure 19. Overfitted material parameters. Young's modulus of concrete reaches upper and lower bounds.

5 DISCUSSIONS

In this study, we explored the system identification process for structural health monitoring using adjoint-based optimization techniques. Our findings highlight the effectiveness of employing high-fidelity Digital Twin models to accurately infer material properties and detect weaknesses in structures. The method has been applied to the "Concerto" bridge with real-world measured displacement. We have found damaged areas that are confirmed by visual inspection of the real state of the bridge.

However, the results are not without limitations. One significant challenge is the dependence on sensor configuration, which can strongly affect the accuracy of the identified material properties. Additionally, the multimodal

DOI: 10.3217/978-3-99161-057-1-158

nature of the optimization problem complicates finding a "true" solution during the identification process, as multiple identified states can yield similar results. Another significant challenge is the convergence criteria, which, on one hand, should stop the optimization process before overfitting the material parameters, and on the other hand, shouldn't stop it too early before all damaged regions are found.

6 OUTLOOK

Moving forward, we recommend several directions for future work:

1) How can we identify the crucial measured locations / optimal sensor placement?
2) How to load the structure? How many load scenarios are required to identify all damaged regions?
3) How can we include the probability of sensor failure and inaccurate measurement?
4) How can we check which damage can be found by a given sensor configuration on the structure?
5) How to circumvent the overfitting of the data?

ACKNOWLEDGMENTS

We would like to acknowledge the funding by the Deutsche Forschungsgemeinschaft (DFG, German Research Foundation) under German's Excellence Strategy - EXC 2163/1 - Sustainable and Energy Efficient Aviation - Project-ID 390881007. NSF grant DMS-2408877, Air Force Office of Scientific Research (AFOSR) under Award NO: FA9550-22-1-0248, and Office of Naval Research (ONR) under Award NO: N00014-24-1-2147. We would like to acknowledge the funding by the Institute of Advanced Studies, Technical University of Munich, under the Hans Fischer Senior Fellowship.

REFERENCES

[1] Airaudo, F. N., Löhner, R., Wüchner, R., and Antil, H., "Adjoint-based determination of weaknesses in structures," Computer Methods in Applied Mechanics and Engineering, Vol. 417, 2023, p. 116471. Doi: 10.48550/arXiv.2303.15329

[2] Antonau, I., Warnakulasuriya, S., Bletzinger, KU. *et al*. Latest developments in node-based shape optimization using Vertex Morphing parameterization. *Struct Multidisc Optim* **65**, 198 (2022). https://doi.org/10.1007/s00158-022-03279-w

[3] Ihar Antonau, Suneth Warnakulasuriya, Roland Wüchner, Facundo Airaudo, Rainald Löhner, Harbir Antil and Talhah Ansari. "Comparison of the First Order Algorithms to Solve System Identification Problems of High-Fidelity Digital Twins," AIAA 2025-0285. AIAA SCITECH 2025 Forum. January 2025.

[4] Rainald Lohner, Facundo Airaudo, Harbir Antil, Roland Wuechner, Suneth Warnakulasuriya, Ihar Antonau and Talhah Ansari. "High-Fidelity Digital Twins: Zooming in on Weaknesses in Structures," AIAA 2025-0286. AIAA SCITECH 2025 Forum. January 2025.

[5] Maboudi, Mehdi & Backhaus, Jan & Ghassoun, Yahya & Khedar, Yogesh & Lowke, Dirk & Mai, Inka & Riedel, Björn & Bestmann, Ulf & Gerke, Markus. (2024). Very High-Resolution Bridge Deformation Monitoring Using UAV-based Photogrammetry. 10.48550/arXiv.2410.18984.

[6] Budelmann, H., Hariri, K., & Holst, A. (2006). A real-scale PC bridge for testing and validating monitoring methods. In Proceedings of the Third International Conference on Bridge Maintenance, Safety and Management, Porto, Portugal.

[7] American Institute of Aeronautics and Astronautics (AIAA), Digital Engineering Integration Committee, "Digital twin: Definition & value," AIAA and AIA Position Paper, 2020. https://www.aiaa.org/docs/default-source/uploadedfiles/ issues-and-advocacy/policy-papers/digital-twin-institute-position-paper-(december-2020).pdf.

[8] National Academies of Science, Engineering, and Medicine, "Foundational research gaps and future directions for digital twins," https://tinyurl.com/cx77p8hd, 2023.

[9] Willcox, K., Ghattas, O., and Soga, K., "Crosscutting Research Needs for Digital Twins," 2024. https://www.santafe.edu/ events/crosscutting-research-needs-digital-twins.

[10] Antil, H., "Mathematical Opportunities in Digital Twins (MATH-DT)," arXiv preprint arXiv:2402.10326, 2024.

[11] Löhner, R., Airaudo, F. N., Antil, H., Wüchner, R., Meister, F., and Warnakulasuriya, S., "High-Fidelity Digital Twins: Detecting and Localizing Weaknesses in Structures," International Journal for Numerical Methods in Engineering, 2024. https://doi.org/10.1002/nme.7568.

[12] Airaudo, F., Antil, H., Löhner, R., and Rakhimov, U., "On the Use of Risk Measures in Digital Twins to Identify Weaknesses in Structures," AIAA SCITECH 2024 Forum, American Institute of Aeronautics and Astronautics, 2024. https://doi.org/10.2514/6. 2024-2622, URL http://dx.doi.org/10.2514/6.2024-2622.

[13] Ansari, T. S. A., R. Löhner, R. Wüchner, H. Antil, S. Warnakulasuriya, I. Antonau, & F. Airaudo (2025). Adjoint-based recovery of thermal fields from displacement or strain measurements. Computer Methods in Applied Mechanics and Engineering 438, 117818, https://doi.org/10.1016/j.cma.2025.117818.

[14] Torzoni, M., Manzoni, A., Mariani, S. (2023). A multi-fidelity surrogate model for structural health monitoring exploiting model order reduction and artificial neural networks. Mechanical Systems and Signal Processing 197, 110376, https://doi.org/10.1016/j.ymssp.2023.110376

[15] Wu, Rih-Teng, and Mohammad Reza Jahanshahi. 2018. "Data Fusion Approaches for Structural Health Monitoring and System Identification: Past, Present, and Future." Structural Health Monitoring 19, no. 2: 553–591. https://doi.org/10.1177/1475921718765174

[16] Kim, J., Lee, S., & Park, H. (2023). Damage detection method using finite element model updating and deep learning for structural dynamic characteristics. Scientific Reports, 13, 18694. https://doi.org/10.1038/s41598-023-46141-9